

Discovery of Charge Density Wave Order in the Topological Insulator Bi_2Se_3

Yanan Li¹, Christian Parsons¹, Sanath Ramakrishna², Anand Dwivedi¹, Marvin Schofield¹, Arneil Reyes², and Prasenjit Guptasarma¹

¹Department of Physics, University of Wisconsin-Milwaukee, Milwaukee, Wisconsin 53211, USA ²National High Magnetic Field Laboratory/Florida State University, Tallahassee, Florida 32310, USA

Abstract

Hexagonally deformed Fermi surfaces and strong nesting, found in topological insulators (TIs) such as Bi_2Se_3 and Bi_2Te_3 over the past decade, have led to several predictions of possible Density Wave order in these systems. Recent evidence for strong Fermi nesting in superconducting $\text{Cu-Bi}_2\text{Se}_3$ and $\text{Nb-Bi}_2\text{Se}_3$ has led to further speculation about the importance of charge order in the context of unconventional superconductivity. Here, we report what we believe is the first direct observation of Charge Density Wave (CDW) order in Bi_2Se_3 . Our results include the observation of a 140K metal-insulator-metal transition in resistivity as a function of temperature. We corroborate this with nuclear magnetic resonance (NMR) studies of the spin-lattice relaxation ($1/T_1$) rate of the ^{209}Bi nucleus, which also displays a transition at 140K. Additionally, we use electron diffraction to reveal a periodic lattice distortion (PLD) in Bi_2Se_3 , together with diffuse charge order between \vec{k} and $\vec{k} \pm \Delta\vec{k}$. This diffuse scattering points toward the presence of an incommensurate charge density wave (I-CDW) above room temperature, which locks into a CDW upon cooling below $\sim 140\text{K}$. We also observe an additional transition in $1/T_1$ near 200K. The transition at 200K appears to display some anisotropy with the direction of applied magnetic field. In this report, we focus on the CDW transition at 140K. We include some speculation of the transition observed at 200K by NMR, also revealed here for the first time.

INTRODUCTION

The 2D layered chalcogenide Bi_2Se_3 and its intercalated versions continue to elicit significant interest due to the presence of non-trivial topological surface states protected by time reversal symmetry, along with fascinating properties of nematic order and superconductivity.¹⁻⁶ Ideally, Bi_2Se_3 is a 3D topological insulator with a single Dirac cone within a substantial bulk energy gap (0.3 eV).⁷ However, several experiments have observed a lowering of the bulk conduction band due to natural electron doping from vacancies or antisite defects crossing the Fermi energy and allowing for bulk electron conduction.⁸⁻¹¹ Under high pressure, or upon intercalating with metals such as Cu and Nb, Bi_2Se_3 displays unconventional superconductivity.¹²⁻¹⁴ Most unconventional superconductivity arises out of strong electron-electron correlations.¹⁵⁻¹⁸ However, Bi_2Se_3 displays weak *sp* electron correlation.^{19,20} This conundrum has led to a search for other possible mechanisms for unconventional electron pairing in Cu-, Sr- and Nb- intercalated Bi_2Se_3 . An idea that has gained ground in recent years is based on Fermi nesting. First principle calculations on $\text{Cu}_x\text{Bi}_2\text{Se}_3$ ¹ in combination with elastic neutron diffraction measurements on $\text{Sr}_{0.1}\text{Bi}_2\text{Se}_3$ ² indicate that singular electron-phonon interactions with strong Fermi nesting at long wavelength can lead to pseudo-triplet pairing with A_{2u} symmetry. In addition to this, there is now strong evidence that with contributions from the bulk, the cross section of the Dirac cone in Bi_2Se_3 evolves from circular geometry at the Dirac point into a hexagon-like geometry around 350 meV above the Dirac point, and eventually to a hexagram-like geometry near 435 meV above the Dirac point.²¹ The near-flat pieces of such a hexagon in the range $0.55E^* < E < 0.9E^*$ can result in nesting vectors at $Q_i = 2k_{\text{Fe}_i}$, $i=1 \dots 3$, where Q_i is the wave vector and k_{Fe_i} is the Fermi momentum.²² Central to a strong Fermi nesting factor is the layered structure of Bi_2Se_3 . Angle-resolved Photoemission Spectroscopy (ARPES) studies on Bi_2Se_3 have confirmed that natural electron-doped Bi_2Se_3 has a hexagonally deformed Fermi Surface. Kuroda et al²¹ have suggested that two flat segments of a hexagonal Fermi surface facing each other across $2\vec{k}_F$ along $\vec{\Gamma} - \vec{k}$ could lead to strong nesting. Realistically, this is a deviation from an ideal TI, which has a single Dirac Cone with a circular Fermi surface,²³ and in which the formation of a charge density wave, or a spin density wave, is forbidden. One of the possible outcomes of such Fermi nesting is the appearance of Density Waves. A few studies have hinted at the existence of CDWs in Cu- Bi_2Se_3 , but so far there has been no evidence of a gap opening with temperature variation, indicating a CDW transition.²⁴⁻²⁶ Additionally, there have been no such reports in Bi_2Se_3 . Here, we report for the first time that Bi_2Se_3 undergoes a transition to a CDW state at 140K.

The ground state of a charge density wave (CDW), which is observed mostly in low dimensional materials, is characterized by spontaneously broken translational symmetry. In the simplest case, the 1D Peierls transition can be a first order or a second order transition, characterized by the temperature evolution of the order parameter. In real life, and in more complex systems, the phase transition to a CDW ground state is mostly observed together with commensurate/incommensurate periodic lattice distortions concomitant with the opening of an energy gap at the Fermi level, resulting in a metal-to-insulator like transition in resistivity as a function of temperature. Single crystals with *imperfect chains* (quasi-1D), or *imperfect nestings* (quasi-2D), can lead to such an energy

gap being partially opened. In such situations, a CDW tends to co-occur with a Periodic Lattice Distortion (PLD)²⁷⁻²⁸ such that the PLD and the CDW are commensurate with the periodicity of the underlying atomic lattice distorted by the PLD. The electronic charge density, which is a scalar quantity and mostly used as an order parameter of a CDW, is coupled with the PLD. In such a situation, the ordered CDW possesses a period that is an integral or a fractional multiple of the period of either the atomic lattice or the PLD. In cases where the CDW periodicity is not represented in the reciprocal lattice by specific vectors \vec{k} , but rather by an entire range of vectors $\vec{k} \pm \Delta\vec{k}$, one observes diffraction patterns with ‘diffuse’ intensity centered around \vec{k} , and often between Bragg reflections, while maintaining the overall symmetry of the underlying lattice. This is a signature of an incommensurate CDW, or I-CDW,²⁷⁻²⁸ which often precedes a CDW transition at lower temperature.

RESULTS

We report here a combination of resistivity, Selected Area Electron Diffraction (SAED) and Nuclear Magnetic Resonance (NMR) studies to reveal that Bi_2Se_3 undergoes a transition to a CDW state at 140K. We observe a 140K metal-insulator-metal transition in resistivity as a function of temperature. Our Nuclear magnetic resonance (NMR) studies of the spin-lattice relaxation ($1/T_1$) rate of the ^{209}Bi nucleus also displays a transition at 140K. Additionally, electron diffraction reveals a periodic lattice distortion (PLD) in Bi_2Se_3 as well as diffuse charge order between \vec{k} and $\vec{k} \pm \Delta\vec{k}$, as described in the previous section. We argue that this diffuse scattering arises from an incommensurate charge density wave (I-CDW) at higher temperature, foreshadowing a transition to CDW order, into which the I-CDW locks upon cooling below $\sim 140\text{K}$. We also identify another transition in NMR $1/T_1$ near 200K. The transition near 200K displays an anisotropy with applied magnetic field. We do not yet have clearly identified physical mechanisms for this additional transition near 200K, and instead focus on our observation of a CDW transition in Bi_2Se_3 at transition temperature $T_d = 140\text{K}$. We provide some speculations about the 200K transition in the discussion section of this paper

Resistivity measurements

Four-probe DC resistivity measurements, shown in Fig. 1 and Fig. 2, were performed in the 2K-300K temperature range with linearly aligned electrodes on the ab surface of Bi_2Se_3 single crystals, and with the electric field $E \parallel ab$. To ensure reproducibility, we performed measurements on several different pieces of as-grown single crystal. Fig. 1a, b, are results on different pieces from the same batch of as-grown single crystal. Resistivity measurements at zero field all show approximately metallic behavior from room temperature down to around 140 K. Note a sharp upturn in resistivity with decreasing temperature, centered around 140K, followed by a return to metal-like behavior below 140K. In Fig. 1a, with cooling, we see a rise in resistivity from $\sim 1.38 \times 10^{-5} \Omega\text{m}$ to $1.47 \times 10^{-5} \Omega\text{m}$; in Fig. 1b, we observe a rise of $\sim 1.31 \times 10^{-5} \Omega\text{m}$ to $1.36 \times 10^{-5} \Omega\text{m}$, followed in both cases by a return to metal-like behavior at lower temperature. The inset to Fig.

1a,b show dp/dT as a function of temperature, clarifying the inflexion point and onset near 140K. We identify this metal-insulator-metal behavior as resulting from a gap or instability at the Fermi level, correlated with a transition to a CDW ground state.^{29,30}

Heating and cooling cycles performed on the second piece of Bi_2Se_3 shown in Fig. 1b display very weak thermal hysteresis behavior above the onset transition temperature 140K, pointing to the possibility that the 140K transition is an unconventional second order CDW transition.^{31,32} On the other hand, the observation of thermal hysteresis (between heating and cooling) in resistivity above 200K, shown as a solid red line and a dashed blue line in Fig. 1b, points to the presence of a possible first order transition at higher temperature. We believe that this could arise from a transition from normal phase to an incommensurate charge density wave phase at some temperature above room temperature.³³ This agrees with our room-temperature electron diffraction data described below, in which we observe the presence of an I-CDW phase. We therefore assign the transition at 140K to a second order transition from I-CDW to CDW. The lack of (or, weak) thermal hysteresis at 140K indicates a possible phonon-mediated unconventional mechanism described further in the discussion section.^{1,2,34,35}

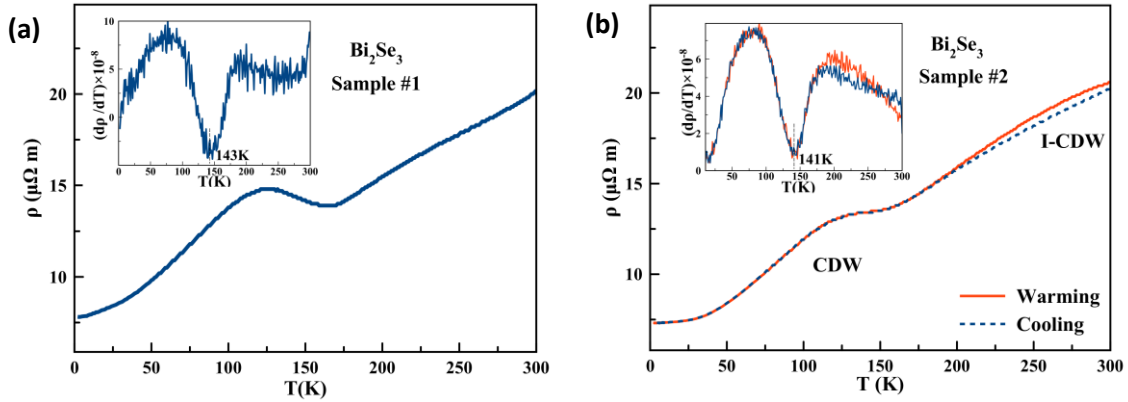


Fig. 1 Resistivity of Bi_2Se_3 as a function of temperature for two different pieces, sample#1 and sample#2, measured in zero magnetic field with the electric field along the ab plane. **a** Measurement on sample #1 while cooling the sample from 300 K to 2 K; **b** Measurement on sample#2 for both cooling and heating. Insets for **a** and **b** are the plots of dp/dT as a function of temperature to clarify the temperature values of the inflexion points and the CDW transition temperature T_d .

Fig. 2 examines the magnetic field dependence of T_d for sample#2, same sample as the one shown in Fig. 1b, with magnetic field $H//c$ -axis varying between 0.00T and 4.50T. The inset in Fig. 2 displays dp/dT as a function of T , indicating that the transition temperature does not change with applied magnetic field H below 5T. This result is similar to the one obtained for an unconventional CDW in $\text{La}_3\text{Co}_4\text{Sn}_{13}$.³¹

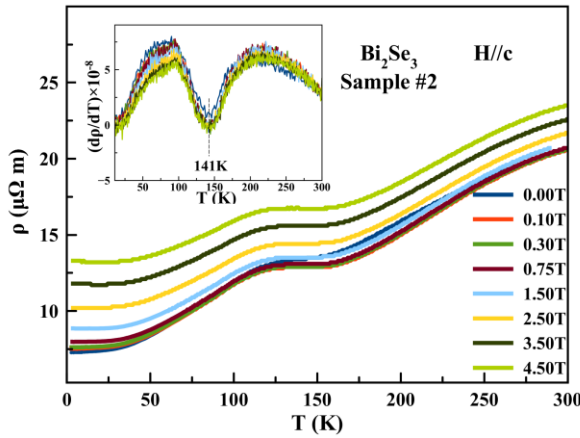


Fig. 2 Thermal dependence of resistivity of Bi_2Se_3 for different values of applied magnetic field $H \parallel c$ -axis varying between 0.00 – 4.50 Tesla.

Electron Diffraction

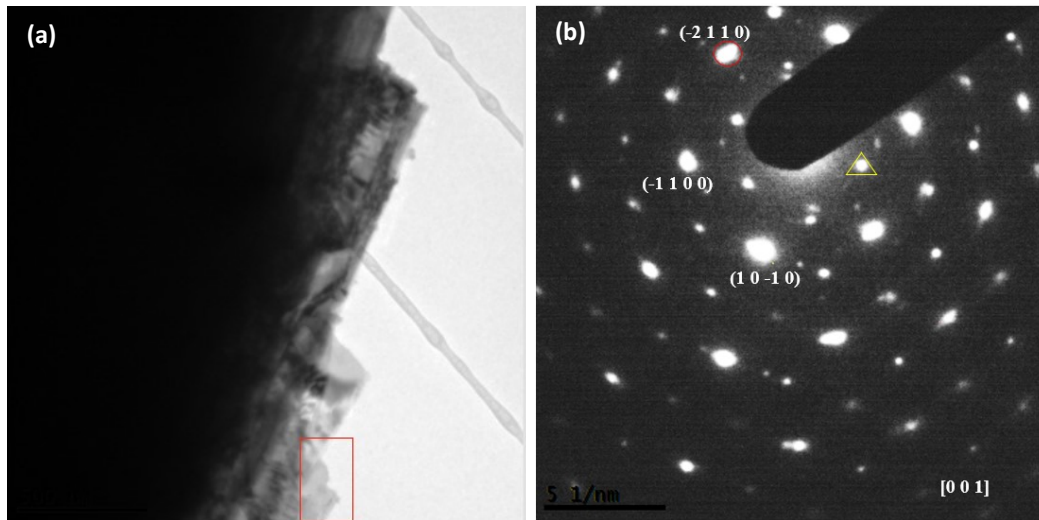


Fig. 3 Transmission Electron Microscopy (TEM) and Selected Area Electron Diffraction (SAED) studies on Bi_2Se_3 single crystal at room temperature. **a** Bright field image of a piece from single crystal of Bi_2Se_3 . The red box indicates the region on which SAED was performed. **b** Electron diffraction along $[001]$ zone axis. Weak reflections of the type identified by a yellow triangle represent normally forbidden reflections from $3a/2$ reflections in the $[001]$ zone axis. Relatively strong reflections, circled in red, are identified reflections from the $[001]$ zone axis.

Fig. 3 and Fig. 4 show Selected Area Electron Diffraction (SAED) performed on Bi_2Se_3 at room temperature. Fig. 3a shows the area from which the diffraction pattern in Figure 3b was obtained along the $[001]$ zone axis. Note, in Fig. 3b, alternate bright and dim spots, with high-intensity spots are identified and circled in red. These features were also observed in SAED by Koski, et al and Wang, et al.^{24,36} Both groups studied the result of intercalation of different zero-valent metals into the van der Waals gaps in Bi_2Se_3 . They suggest that the most likely reason for the appearance of these weak intensity spots, otherwise forbidden in the cubic-like ABC $[001]$ zone axis in the host Bi_2Se_3 lattice, is the result of a stacking fault. In other words, the presence of zero-valent intercalants in the Van der Waals gap can alter interplanar energetics in such a way as to stabilize

hexagonal stacking relative to rhombohedral stacking, resulting in a high density of stacking faults. Based on our XRD results of an increase in c-axis length (in the later discussion), and our evidence for stacking faults in SAED, we suggest that the Van der Waals gaps in our Bi_2Se_3 crystals have zero-valent Bi or Se metal resulting from “self-intercalation.” The process of self-intercalation has previously been discussed by several other authors.^{37,38}

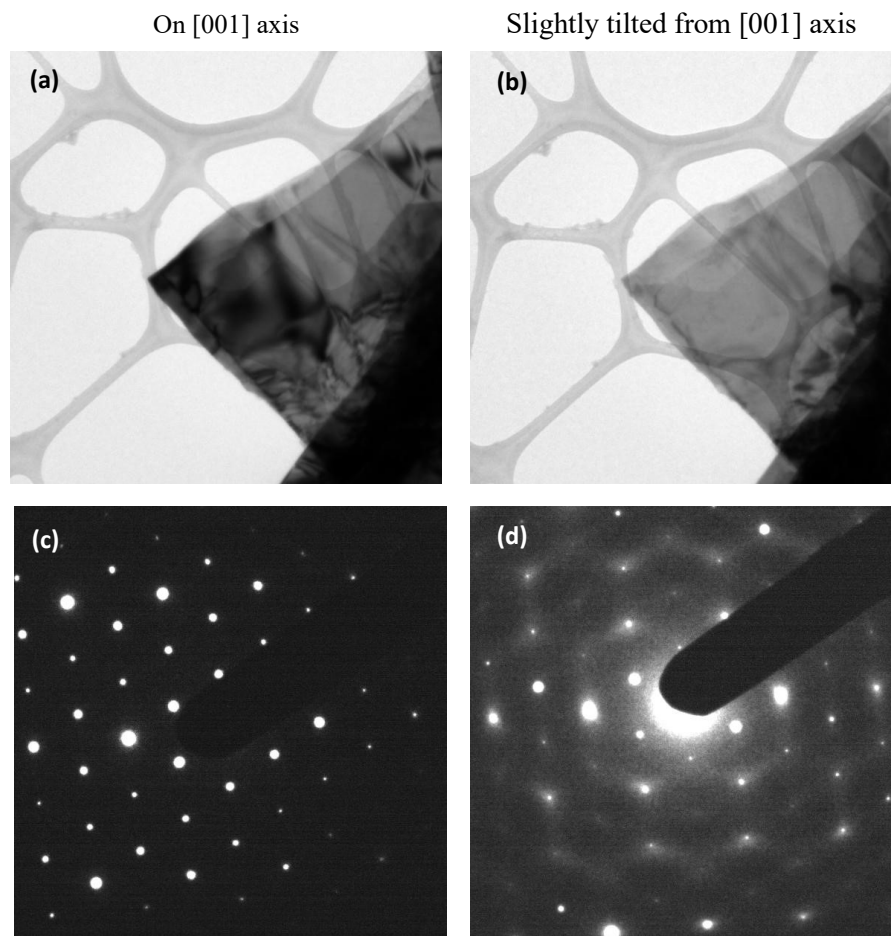
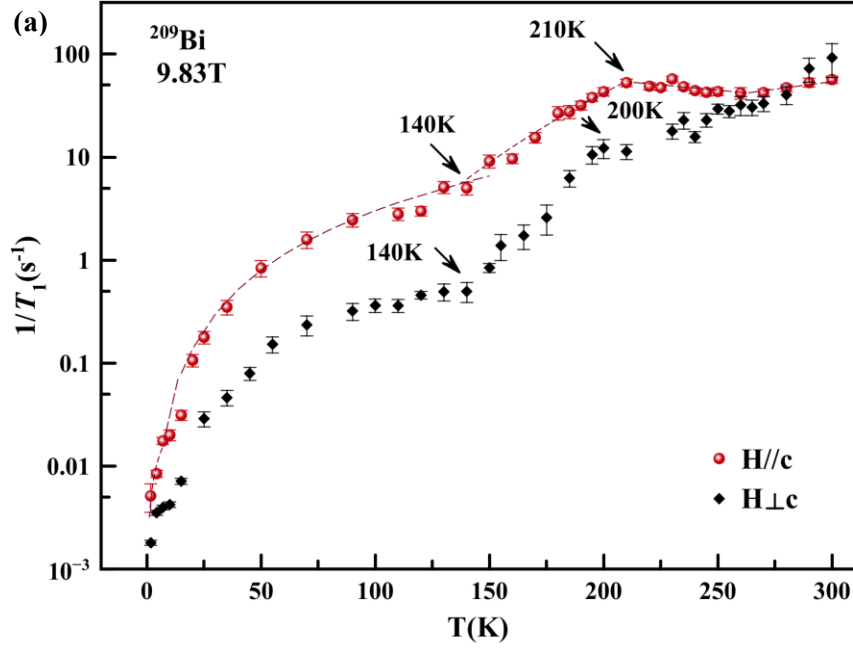


Fig. 4 **a, b** Bright field TEM on a flake obtained from single crystal Bi_2Se_3 . **c, d** Selected Area Electron Diffraction from the corresponding areas shown in (a) and (b). The images in (a) and (c) show results when the beam is on $\langle 001 \rangle$ axis. Images in (b) and (d) show off-axis electron diffraction, for which the sample was tilted slightly (less than 5 degrees) away from zone axis.

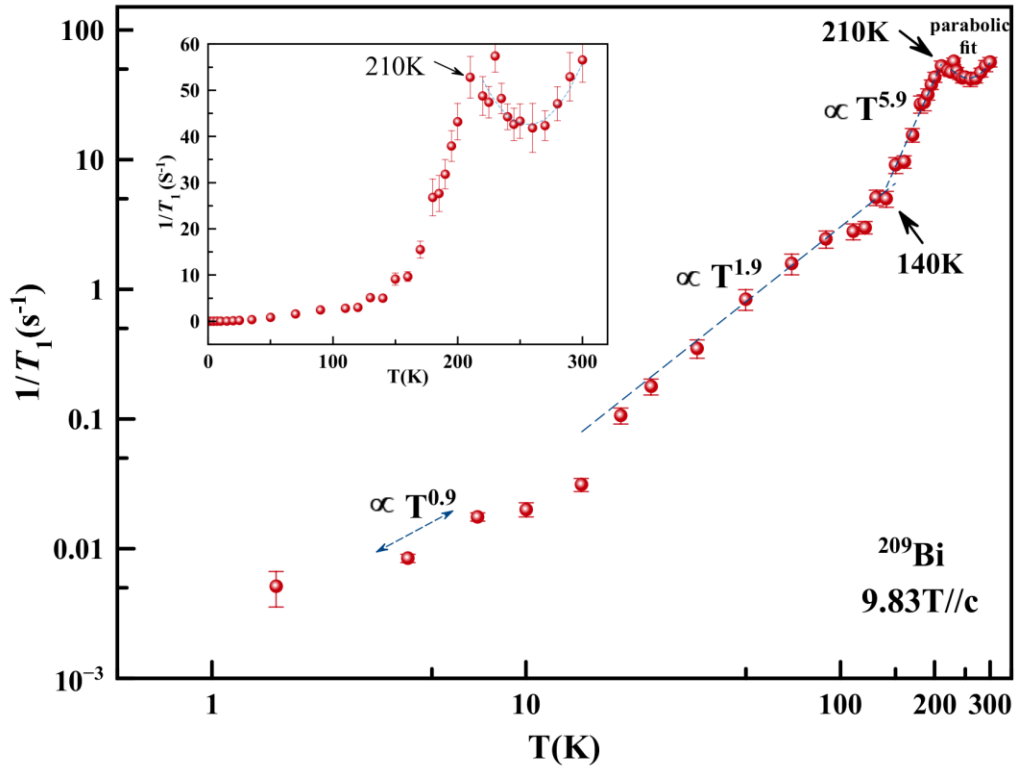
Fig. 4 displays bright field TEM and SAED on flakes obtained from single crystal Bi_2Se_3 . Fig. 4a, c are bright field images on the $\langle 001 \rangle$ zone axis. Fig. 4b, d are taken from the same region of the flake, with the sample tilted slightly (less than 5 degrees) away from the zone axis. The images in Fig. 4c, d correspond to the areas shown in Fig. 4a, b, respectively. As can be seen in Fig. 4d, the diffraction pattern with the crystal tilted

slightly off the $\langle 001 \rangle$ zone axis yields diffuse streaks between the diffraction spots. As discussed in previous reports on other similar layered compounds,^{27-28, 39-42} we interpret that this diffuse intensity is due to Periodic Lattice Distortion (PLD) associated with an incommensurate charge density wave (I-CDW), which often occurs as a precursor to a charge density wave (CDW), as we discuss further below.

Nuclear Magnetic Resonance



(b)



(c)

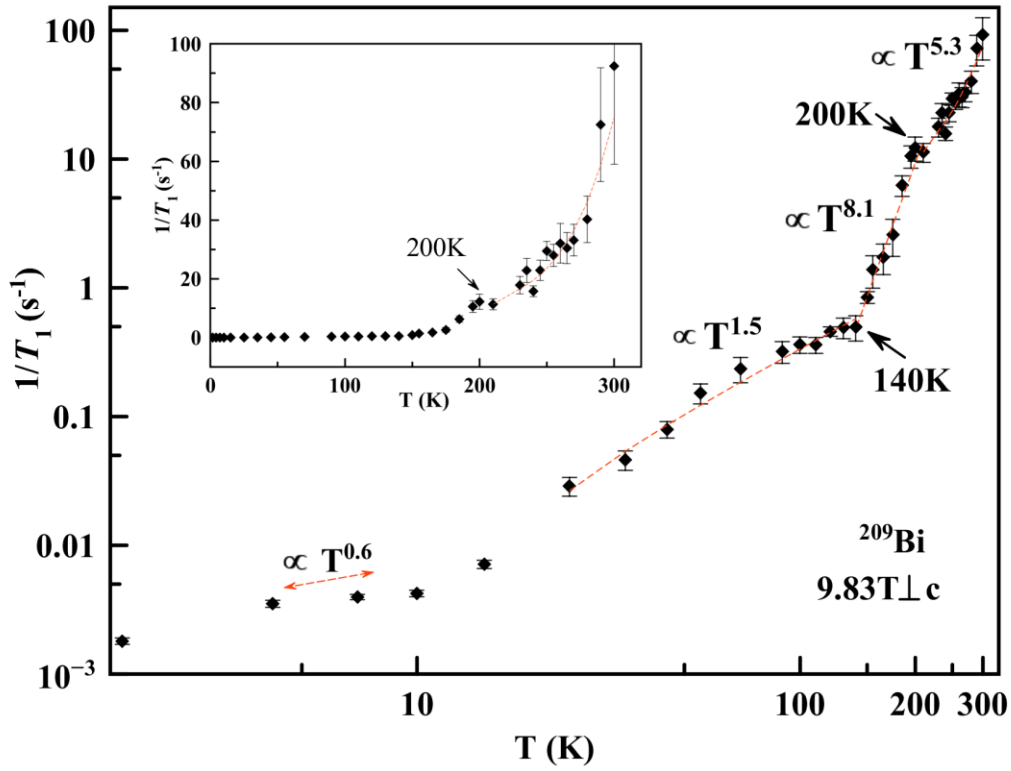


Fig. 5 Spin-lattice relaxation rate ($1/T_1$) shown with temperature T varying between 1.6K and 300K. **a** Linear scale x, Logarithmic scale y, with magnetic field directions: $H \parallel c$ -axis (red solid ball) and $H \perp c$ -axis (black diamond). **b** Logarithmic scale x y, for $H \parallel c$ -axis and **c** $H \perp c$ -axis with Power-Law fitting, while except 220K to 300K in $H \parallel c$ direction was fitted by a parabola. Arrows indicate possible transitions at 140K and 200K. Inner graphs for **b** and **c** are the Linear-Linear plots for $H \parallel c$ -axis and $H \perp c$ -axis.

Fig. 5a shows the temperature dependence of the nuclear spin-lattice relaxation rate ($1/T_1$) with varying temperature (1.6K to 300K) with the external magnetic field applied in two orientations, $H \parallel c$ -axis and $H \perp c$ -axis at $H = 9.83$ T, in which Fig.5a displays Log y, linear-x for both directions, Fig.5b and Fig.5c displays Log y, Log x in each direction. The $1/T_1$ for both orientations as a function of temperature follows a similar behavior except that the relaxation rates for $H \parallel c$ is about an order of magnitude longer compared to $H \perp c$, but they approach almost the same value at room temperature.

The $1/T_1$ was fitted by standard expression for spin 9/2 nuclei to fit the magnetization recovery $M(t)$. The results of this fit are shown in Fig. 5, where we see two obvious slope changes: at 140K and at 200K, indicated by arrows. We repeated our measurements between 130K and 300K in order to confirm the inflection observed near 200K. The 140K anomaly coincides with the metal-insulator-metal transition observed in our resistivity measurements. For this reason, we assign the 140K transition to a CDW transition. It is interesting that the 200K transition displays a weak anisotropy with applied magnetic field. To understand this further, we present Fig. 5 b and c, which displays the exponents of T in three different temperature regimes: 20K-140K, 140K-200K, and 200K-300K.

DISCUSSION

The exact nature of Fermi surface distortion, nesting, and density wave instability in a system such as Bi_2Se_3 is critically dependent upon the details of its fermiology. Correlated electron systems typically exhibit intertwined electronic ordered states resulting from several degrees of freedom such as lattice, charge, dimensionality, nematicity, and spin – all of which, in turn, tend to be strongly materials-dependent. Thus, many properties of chalcogenides such as Bi_2Se_3 arise from the nature of fluctuations, or overlaps in order parameter, among such intertwined orders. The severity of the overlap tends to be materials-dependent as well. Below, we discuss how materials aspects of Bi_2Se_3 , specifically, can lead to multiple ground states such as that of a charge density wave (CDW). Further, the proximity of superconductivity and density wave orders in many materials begs a discussion of the observed CDW in the context of superconductivity in Bi_2Se_3 , which we think is critical to the understanding of charge order, superconductivity, as well as nematicity.⁴³ In this section, we begin with a discussion of the two different transitions found in our measurements. We end by describing important materials considerations which, we believe, drive the multiple (possibly intertwined) order parameters in this layered chalcogenide.

Transition near 140 K:

Nuclear Magnetic Resonance measurements, in Fig. 5, together with resistivity measurements in Fig. 1 and Fig. 2 clearly reveal a transition near 140K. We identify this as a transition to a CDW state below 140K. We support this conclusion from electronic diffraction measurements at room temperature (Fig. 3 and Fig. 4), which reveal the presence of a periodic lattice distortion (PLD), combined with diffuse scattering in off-axis diffraction, suggesting the presence of an incommensurate charge density wave (I-CDW) at room temperature. Interestingly, T_1 anomalies have been associated with CDW transition in layered systems.⁴⁴⁻⁴⁷ This originates from the lattice distortion induced by CDW which changes the electronic field gradient on the nuclear site. The magnitude of this change is related to the strength of coupling between the nuclear quadrupole moment and the electric field gradient (EFG). Contrary to Young et al,⁴⁸ we believe that the quadrupolar relaxation due to fluctuating EFG dominates the relaxation as it undergoes the CDW state.

Transition near 200K:

Given that the behavior of $1/T_1$ is dependent upon the details of the high temperature phonon spectrum, one would expect it to behave differently above and below the Debye temperature. For Bi_2Se_3 , Debye temperature is $\Theta_D \approx 182\text{K}$. Thus, it is plausible that the transition observed around 200K in Fig. 5 is due to changes in the phonon spectrum across Θ_D .

Note the anisotropy in this transition with the direction of applied magnetic field, $H//c$ and $H \perp c$, as shown in Fig.5b,c. According to our fits, $1/T_1$ for $H//c$, yields an exponent of $T^{5.9}$ for $140\text{K} < T < 210\text{K}$ and a parabola dependence for $210\text{K} < T < 300\text{K}$. For $H \perp c$, $1/T_1$ has a $T^{8.1}$ dependence for $140\text{K} < T < 200\text{K}$ and a $T^{5.3}$ dependence for $200\text{K} < T < 300\text{K}$.

In Fig.1b, we observe a thermal hysteresis in resistivity above 182K. Whereas a transition across Θ_D would yield a change in slope of resistivity, we are hard-pressed to explain the thermal hysteresis in resistivity, for $T > 182\text{K}$, based purely on a Debye temperature transition. A hysteresis between heating and cooling is often observed below a first-order I-CDW to CDW transition. Occasionally, one does not observe a thermal hysteresis, as in the case of $\text{Lu}_5\text{Ir}_4\text{Si}_{10}$. In such cases, other authors tend to suggest that the transition either is of second order or has some “unconventional” origin^{31,32}. In our case, as shown in Fig 1b, the resistivity below 140K does not display a thermal hysteresis. This indicates that the 140K transition is likely a second-order CDW transition. If this reasoning is correct, the 200K transition is a first-order transition.

In the end the fundamental origin of the transition near 200K is unclear. There are two possible mechanisms: one based on a 182K Debye temperature transition, and a second

based on the nature of the I-CDW. Additional work is needed in order to differentiate one mechanism from the other.

We also note that in Fig. 5 the $1/T_1$ data for both orientations follow similar behavior as a function of temperature except that the relaxation rates for $H//c$ is about an order of magnitude faster compared to $H \perp c$. However, they approach almost the same value at room temperature. Above 200K, the temperature behavior differs: the $1/T_1$ value remains constant from room temperature to 200K for the parallel case while it precipitously drops for the perpendicular case. It is as if there is a constant relaxation mechanism that only exists in the parallel direction and is independent of temperature, while in the perpendicular direction, this mechanism gradually diminishes until the temperature reaches 200K. The origin of this mechanism is not clear but it may be related to the topological nature of this system which suppresses the relaxation channel when the field is applied parallel to the planes.⁴⁹⁻⁵⁰

At low temperature, $T < 15K$, the spin relaxation rate reveals an almost-linear behavior of $T^{0.9}$ for $H//c$. This indicates a metallic Korringa-type behavior in our sample, $1/T_1 \propto D^2(E_F)T$, where $D^2(E_F)$ is the density of states, and where relaxation is dominated by conduction electron scattering. This is contrast with that observed by Young et al⁴⁸ for $H//c$ in their sample #3 which was grown using a self-flux method similar to ours, but quenched from a lower temperature. Our results at $H \perp c$ show a $T^{0.6}$ behavior in this temperature range.

The case for a Charge Density Wave in Bi₂Se₃

As discussed earlier, topological insulators such as Bi₂Se₃ and Bi₂Te₃ are expected to host density wave order due to their complex fermiology – in particular, strong Fermi surface nesting.^{21,22} Angle Resolved Photoemission Spectroscopy (ARPES) measurements show that Bi₂Se₃ has a hexagonally deformed Fermi surface. The two parallel segments in the hexagonal Fermi surface separated by $2k_F$ (where, k_F is the Fermi wavevector) can lead to strong nesting and density wave order. Given the topology of the surface states, the two parallel vectors \vec{k} and $-\vec{k}$ could also yield a spin density wave (SDW). However, the Fermi surface is deformed only above 200meV, where bulk bands can become involved. Below 200meV, one finds a pure surface state with a circular constant energy contour.²¹ Thus, bulk states may contribute to Fermi surface deformation, leading to strong Fermi nesting. Shubnikov-de Haas measurements on Nb-Bi₂Se₃ have revealed evidence for a small extra Fermi pocket besides the main Fermi surface of Bi₂Se₃.³ Additionally, a first-principles linear response calculation for Cu-Bi₂Se₃ has revealed a ‘prism-like’ fermi pocket at the Γ point, with opportunities for strong Fermi nesting.¹ Thus, theoretically speaking, the CDW transition reported here is not a surprising result.

When intercalated with Nb, Cu, or Sr, and when subjected to high pressure, Bi₂Se₃ becomes a superconductor with unconventional pairing.^{2,12-14} Strong electron correlations are often found in the vicinity of superconductivity^{17,18} – however *sp* electrons in Bi₂Se₃

are weakly correlated. Xiangang and Sergey¹ suggest that unconventional superconductivity in intercalated layered systems such as Cu-Bi₂Se₃ might arise from an enhancement of electron-phonon coupling due to strong nesting at long wavelengths. At a certain wave vector q_0 , all pairing channels become degenerate and compete with each other. This singular electron phonon interaction with strong Fermi nesting at long wavelength can provide a large effective coupling constant favoring pseudo-triplet pairing of A_{2u} symmetry in intercalated Bi₂Se₃.¹ Thus, an interplay of strong spin-orbit coupling, unbroken time-reversal symmetry, and inversion symmetries with certain lattice distortions could lead to enhanced electron-phonon correlations and exotic superconducting states.

As described by Zhu et al⁵¹, the origin of CDW is strongly related to dimensionality. They describe “Type-I” CDWs as quasi-1D systems with origins in traditional Peierls’ instability and Fermi Surface Nesting (FSN), with lattice distortion being a consequence of the electronic disturbance, as found in linear-chain compounds. Zhu et al assert that “Type-II” CDWs, in contrast, are driven by electron-phonon coupling (EPC) and not by FSN. In such case, the electronic and lattice instabilities are intimately tied to each other with a phonon mode at q_{CDW} which goes to zero at the transition temperature T_d . This second type does not require a metal-insulator transition associated with T_d . They further describe a “Type-III” case, where a charge modulation is found without the driving force of an FSN or EPC, and where the driving force is possibility electron correlations.

Most CDW occurs in quasi-1D or quasi-2D; our current understanding of CDW does not include all the complexities involved in the 3D case, where electron correlations are thought to play a primary role.⁵¹ In this context, it is instructive to further discuss the possible effect of intercalation on k_F anisotropy between k_z versus k_x , k_y . Xiangang and Sergey¹ suggest that small changes in the position of Bi in the z-direction can modify the nesting vector $X(q) = \sum \delta(\epsilon_k) \delta(\epsilon_{k+q})$, where, ϵ_k and ϵ_{k+q} are the energy of states at/near the Fermi level. This nesting vector is largest for wavevector q along the Γ_z direction, when q is close to zero. This can lead to strong Fermi nesting, and strong electron-phonon coupling. Displacement along [001] at small qs (i.e., small momenta) breaks spatial inversion symmetry, lifts double degeneracy, and leads to a large electron-phonon coupling matrix element along this direction close to zone center. Further calculations by Xiangang and Sergey¹ and neutron scattering experiments by J. Wang, et al² show broad phonon linewidths for small qs , which could dominate electron-phonon coupling. Based on these arguments, we tentatively pose the possibility of the presence of a quasi-1D Peierls-type transition in the z-direction of Bi₂Se₃.

Electron Diffraction

Room temperature selected area electron diffraction in Figures 2b, 3c, and 3d, taken along the $\langle 001 \rangle$ zone axis, displays the hexagonal symmetry that Bi₂Se₃ is known for. This is indicated by labeled diffraction spots. Figures 2a, 3a, 3b are bright field

Transmission Electron Microscopy images showing the portions of the single crystal where the convergent electron beam was placed. Note the image in Fig. 3d, for images tilted slightly from zone axis. This clearly shows diffuse stripes between diffraction spots. As also discussed earlier, such diffuse scattering arises from incommensurate lattice distortion concomitant with an incommensurate charge density wave (I-CDW). We use this information, together with our observation of the opening up of a gap near 140K in two bulk measurements (resistivity and NMR T_1) as evidence for a CDW transition at 140K.

Materials considerations

The somewhat elusive nature of superconductivity in single crystals of Cu-Bi₂Se₃, especially the variability of superconducting fraction and T_c to quenching temperature^{25,26}, is likely due to the high sensitivity of electron interactions to actual conditions of quenching and growth. The crystals discussed here were grown using a standard self-flux method, and a quenching temperature of 650C. The ideal topological insulator, Bi₂Se₃, has separate bulk and surface states. However, experimentally, intrinsic defects and disorder can be widely found in Bi₂Se₃³⁷ and intercalated/electron-doped Bi₂Se₃⁹. Schneeloch et al²⁶ used different growth conditions to grow Cu doped Bi₂Se₃ superconductor and reported that high temperature quenching (above 560C) is essential for superconductivity, especially superconductivity with high diamagnetic shielding fraction. Other growth conditions either cause no SC or weak diamagnetic shielding fraction. This is also our observation²⁵ in Cu-Bi₂Se₃. Schneeloch et al suggest that the quenching process either helps maintain a primary intercalated phase or a secondary phase responsible for superconductivity. Huang et al show that high annealing temperature (~600C) can cause intercalation of Bi₂ in Bi₂Se₃.³⁵ Our results indicate that high-temperature quenching (above 650C) leads to strong electron and lattice order, and to interesting electronic ground states such as a CDW or superconductivity.

X-ray diffraction (XRD), shown in supplementary data, reveals that the a-axis value of our Bi₂Se₃ agrees with those of most other reports, but that the c-axis, at 28.66 Å, is 0.02 Å higher than the 28.64 Å reported in most previous reports Bi₂Se₃.^{37,52-53} Huang et al assert that a longer c-axis arises from unintentionally doped Bi-rich flux growth of Bi₂Se₃ where Bi forms a neutral metal Bi₂ layer intercalated into the van der Waals gap.³⁷ They also show that crystals with patches of intercalated Bi show high c-axis values of up to 28.65 Å, close to the c-axis value of 28.66 Å obtained from our Rietveld refinement. XRD results on our Bi₂Se₃ single crystals show no signs of the formation of metastable phases of staged (Bi₂)_m(Bi₂Se₃)_n. The solidification temperature of Bi₂Se₃ (705 C) is higher than the melting point of both pure Bi (271.4 C) and pure Se (220 C). Additionally, Se is a vapor above 685 C, which is below the solidification temperature of Bi₂Se₃. Consequently, the stoichiometry of Bi₂Se₃ forming at the liquid-vapor interface can be highly dependent upon the vapor pressure of Se at 705 C. For high annealing temperature (around 600 C), partial decomposition might occur. Huang presumes that this is due to a large number of Se vacancies created in an evacuated environment,

resulting in liquid Bi in the flux ending up in the Van der Waals gaps rather than incorporating into a Bi-Se quintuple layer containing Se vacancies. Our crystals, quenched at 650 C (above the high annealing temperature of 600 C that Haung claims results in Se vacancies) could lead to Se vacancies and intercalated Bi.

We surmise that, as there is not enough excess Bi to form the metastable phase of staged $(\text{Bi}_2)_m(\text{Bi}_2\text{Se}_3)_n$, excess Bismuth in our crystals forms randomly distributed Bi_2 inter-layers in the crystal. The resulting Bi-chains could help form a quasi-1D Peierls-type transition or a quasi-2D type CDW.^{37, 51, 54} In summary, specific growth conditions are critical to the observation of a CDW or superconductivity in Bi_2Se_3 .

To conclude, we present evidence for the first experimental observation of charge density wave (CDW) order in Bi_2Se_3 . Diffuse streaks in SAED measurements indicate the presence of an incommensurate periodic lattice distortion at room temperature together with diffuse streaks reminiscent of an incommensurate charge density wave (I-CDW). A metal to insulator transition at 140K in resistivity measurements indicates the opening of a CDW-like energy gap. NMR $1/T_1$ measurements further confirm this 140K transition. Using this, together with thermal hysteresis studies of resistivity, we conclude that Bi_2Se_3 displays an unconventional second-order CDW transition temperature at 140K. NMR also reveals another transition near 200K. The 200K transition is not as clear – we discuss the possibility that this could be sensing a transition across the Debye temperature Θ_D in Bi_2Se_3 , or a transition to a first-order incommensurate CDW. We also discuss how our growth methods promote the formation of a CDW. We suggest that strongly correlated ground states are present in Bi_2Se_3 crystals grown with a high annealing and quenching temperature. In this scenario, the higher temperature growth conditions result in self-intercalation of Bi into Bi_2Se_3 , producing in turn a Charge Density Wave transition. Thus, our results suggest a strong dependence of electronic correlations on growth conditions and to the occurrence of ground states such as CDW and superconductivity.

METHODS

Single crystals of Bi_2Se_3 were prepared by melting high purity (99.999%) powders of Bi and Se. Stoichiometric mixtures of 2.5 g were sealed into high-quality quartz tubes in vacuum after being weighed and sealed in an inert glove box, taking extreme care to never expose to air. The mixtures sealed in quartz tubes were heated up to 850 C and held for 20 hours. They were then cooled to 650 C at 0.1 C/min, followed by quenching into ice- water from high temperature. This yielded large, shiny single crystals which were easily cleaved along the ab plane.

Powder X- ray diffraction data were collected from pieces of single crystals powdered inside an inert glove box. Rietveld refinement was performed using GSAS (General Structure Analysis System) and the EXPGUI interface. Selected Area Electron Diffraction (SAED) was performed at room temperature with a Hitachi H-9000NAR high

resolution transmission electron microscope (HRTEM) operated at 300 kV. 4-probe resistivity measurements were performed with varying temperature and magnetic field using a Quantum Design Physical Property Measurement System (PPMS).

Pulsed ^{209}Bi NMR (Nuclear Magnetic Resonance) measurements were performed on a Bi_2Se_3 single crystal of crystal size $\sim 0.94 \times 0.58 \times 0.41$ cm placed inside a home-built probe in an 11-Tesla Helium cryostat. The single crystal of Bi_2Se_3 was studied with magnetic field oriented in two directions, H \parallel c and H \perp c. Spin-echo signals for ^{209}Bi NMR spectra were processed using the summed Fourier transform method, with field swept from 9.7T to 10.5T. Spin Lattice relaxation time T_1 measurements in both H \parallel C and H \perp C directions were performed at stabilized temperature points varying between 1.6K and 300K, with saturation pulses and typical time delays of 130ms $1/T_1$ measures the recovery of the longitudinal nuclear magnetization following an external perturbation such as an RF field. Following Nisson,⁵⁵ we applied the standard expression for spin 9/2 nuclei to fit the magnetization recovery $M(t)$ of the central $m=\pm 1/2$ nuclear transition, as follows:

$$M(t)=M_0-2f\left(\frac{7938}{12155}e^{-45t/T_1} + \frac{1568}{7293}e^{-28t/T_1} + \frac{6}{65}e^{-15t/T_1} + \frac{24}{715}e^{-6t/T_1} + \frac{1}{165}e^{t/T_1}\right),$$

Here, M_0 is the equilibrium magnetization and f is the inversion fraction.

REFERENCES

- [1] Wan, X. & Savrasov, S. Turning a band insulator into an exotic superconductor. *Nat Commun* **5**, 4144 (2014).
- [2] Wang, J. *et al.* Evidence for singular-phonon-induced nematic superconductivity in a topological superconductor candidate $\text{Sr}_{0.1}\text{Bi}_2\text{Se}_3$. *Nat Commun* **10**, 2802 (2019).
- [3] Lawson, B. J. *et al.* Multiple Fermi surfaces in superconducting Nb-doped Bi_2Se_3 *Phys. Rev. B* **94**, 041114(R) (2016).
- [4] Hecker, M. & Schmalian, J. Vestigial nematic order and superconductivity in the doped topological insulator $\text{Cu}_x\text{Bi}_2\text{Se}_3$. *npj Quant Mater* **3**, 26 (2018).
- [5] Matano, K. *et al.* Spin-rotation symmetry breaking in the superconducting state of $\text{Cu}_x\text{Bi}_2\text{Se}_3$. *Nature Phys* **12**, 852–854 (2016).

- [6] Shen, J. *et al.* Nematic topological superconducting phase in Nb-doped Bi₂Se₃. *npj Quant Mater* **2**, 59 (2017).
- [7] Xia, Y. *et al.* Observation of a large-gap topological-insulator class with a single Dirac cone on the surface. *Nature Phys* **5**, 398–402 (2009).
- [8] Hsieh, D. *et al.* A tunable topological insulator in the spin helical Dirac transport regime. *Nature* **460**, 1101–1105 (2009).
- [9] Hor, Y. S. *et al.* p-type Bi₂Se₃ for topological insulator and low-temperature thermoelectric applications. *Phys. Rev. B* **79**, 195208 (2009)
- [10] Tumelero M. A., Faccio R. & Pasa A. A. The role of interstitial native defects in the topological insulator Bi₂Se₃. *Physics: Condensed Matter* **28**, 425801 (2016).
- [11] Lahoud, E. *et al.* Evolution of the Fermi surface of a doped topological insulator with carrier concentration. *Phys. Rev. B* **88**, 195107 (2013)
- [12] Kirshenbaum, K. *et al.* Pressure-Induced Unconventional Superconducting Phase in the Topological Insulator Bi₂Se₃. *Phys. Rev. Lett.* **111**, 087001 (2013).
- [13] Sasaki, S. *et al.* Topological Superconductivity in Cu_xBi₂Se₃. *Phys. Rev. Lett.* **107**, 217001 (2011)
- [14] Asaba, T. *et al.* Rotational Symmetry Breaking in a Trigonal Superconductor Nb-doped Bi₂Se₃. *Phys. Rev. X* **7**, 011009 (2017)
- [15] Kohama, Y. *et al.* Possible Unconventional Superconductivity in Iron-Based Layered Compound LaFePO: Study of Heat Capacity. *J. Phys. Soc. Jpn.* **77**, 094715 (2008)
- [16] Kiss, T. *et al.* Photoemission Spectroscopic Evidence of Gap Anisotropy in an f-Electron Superconductor. *Phys. Rev. Lett.* **94**, 057001
- [17] Stewart, G. R. Unconventional superconductivity. *Advances in Physics*, **66**, 75-196 (2017)
- [18] Davis, J. C. S. & Lee, D.-H. Concepts relating magnetic interactions, intertwined electronic orders, and strongly correlated superconductivity. *Proc. Natl Acad. Sci. USA* **110**, 17623–17630 (2013)
- [19] Biswas, D., Thakur, S., Balakrishnan, G. & Maiti, K. Exceptional surface and bulk electronic structures in a topological insulator, Bi₂Se₃. *Sci Rep* **5**, 17351 (2015).
- [20] Hor, Y. S. *et al.* Superconductivity in Cu_xBi₂Se₃ and its implications for pairing in the undoped topological insulator. *Phys. Rev. Lett.* **104**, 057001 (2010).

- [21] Kuroda, K. et al. Hexagonally Deformed Fermi Surface of the 3D Topological Insulator Bi_2Se_3 . *Phys. Rev. Lett.* **105**, 076802 (2010).
- [22] Fu, L. Hexagonal Warping Effects in the Surface States of the Topological Insulator Bi_2Te_3 . *Phys. Rev. Lett.* **103**, 266801 (2009).
- [23] Zhang, H., Liu, C.-X., & Zhang, S.-C. Spin-Orbital Texture in Topological Insulators. *Phys. Rev. Lett.* **113**, 066801 (2013).
- [24] Koski, K. J. et al. Chemical intercalation of zerovalent metals into 2D layered Bi_2Se_3 nanoribbons. *JACS* **134**, 13773–13779 (2012).
- [25] Smith, Nathaniel P., "Crystal Growth and Manipulation of Intercalated Chalcogenides as Superconductors and Topological Insulators" PhD Thesis, University of Wisconsin Milwaukee (2018).
- [26] Schneeloch, J. A., Zhong, R. D., Xu, Z. J., Gu, G. D., and Tranquada, J. M., Dependence of superconductivity in $\text{Cu}_x\text{Bi}_2\text{Se}_3$ on quenching conditions. *Phys. Rev. B* **91**, 144506 (2015)
- [27] Wilson, J. A., Di Salvo, F. J. & Mahajan, S. Charge-density waves and superlattices in metallic layered transition-metal dichalcogenides. *Adv. Phys.* **24** 117–201(1975)
- [28] Wilson, J. A., Di Salvo, F. J. & Mahajan, S. Charge-density waves in metallic, layered, transition-metal dichalcogenides. *Phys. Revs. Lett.* **32** 882 (1974)
- [29] Duvjir, G. et al. *Emergence of a Metal–Insulator Transition and High-Temperature Charge-Density Waves in VSe_2 at the Monolayer Limit*. *Nano Letters* **18** (9), 5432–5438 (2018)
- [30] Craven, R. A. & Meyer, S. F., Specific heat and resistivity near the charge-density-wave phase transitions in 2H-TaSe_2 and 2H-TaS_2 . *Phys. Rev. B* **16**, 4583 (1977)
- [31] Welsch, J. et al. Second-order charge-density-wave transition in single crystals of $\text{La}_3\text{Co}_4\text{Sn}_{13}$. *Phys. Rev. Materials* **3**, 125003 (2019)
- [32] Kuo, Y.-K., Lue, C. S., Hsu, F. H., Li, H. H. & Yang, H. D. Thermal properties of $\text{Lu}_5\text{Ir}_4\text{Si}_{10}$ near the charge-density-wave transition. *Phys. Rev. B* **64**, 125124 (2001)
- [33] Zong, A. et al. Ultrafast manipulation of mirror domain walls in a charge density wave. *Sci. Adv.* **4**, 5501 (2018).
- [34] Wezel, J. V., Nahai-Williamson, P., and Saxena S.S. Exciton-phonon-driven charge density wave in TiSe_2 . *Phys. Rev. B* **81**, 165109 (2010).

- [35] Sugawara, K. et al. Unconventional charge-density-wave transition in monolayer 1T-TiSe₂. *ACS Nano* **10**, 1341 (2015).
- [36] Wang, M. & Koski, K. J. Polytypic phase transitions in metal intercalated Bi₂Se₃. *J. Phys. Condens. Matter* **28**, 494002 (2016).
- [37] Huang, F.-T. et al. Nonstoichiometric doping and Bi antisite defect in single crystal Bi₂Se₃. *Phys. Rev. B* **86**, 081104(R) (2012).
- [38] Dai, J. et al. Toward the Intrinsic Limit of the Topological Insulator Bi₂Se₃. *Phys. Rev. Lett.* **117**, 106401(2016)
- [39] Williams, P. M., Scruby, C., Clark, W. & Parry, G. Charge density waves in the layered transition metal dichalcogenides. *J. Phys. Colloques.* **37** C4-139–150(1976)
- [40] McMillan, W. L. Landau theory of charge-density waves in transition-metal dichalcogenides. *Phys. Rev. B* **12** 1187 (1975)
- [41] Di Salvo, F. J. & Maurice Rice, T. Charge-density waves in transition-metal compounds *Phys. Today* **32** 32 (1979)
- [42] Li, Y., Smith, N. P., Rexhausen, W., Schofield, M. A. & Guptasarma, P. Possible lattice and charge order in Cu_xBi₂Te₂Se. *J. Phys. Mater.* **3** 015008 (2020)
- [43] Séamus Davis, J. C. & Lee, D.-H. Concepts relating magnetic interactions, intertwined electronic orders, and strongly correlated superconductivity. *PNAS.* **110**, 17623-17630 (2013)
- [44] Berthier, C., Jérôme, D., Molinié, P. *J. Phys. C: Solid State Physics*, **11**, 797 (1978)
- [45] Ohno, T., Kishimoto, Y., Miyatani, K. *Physica B (Amsterdam)* 230, 988 (1997)
- [46] Tsuda, T., Kitaoka, Y., Yasuoka, H. *Physica B+C (Amsterdam)* 105, 414 (1981)
- [47] Wada, S., Alloul, H., Molinié, P. *J. Physique Lett.* **39**, 243-247 (1978) Proton spin-lattice relaxation time in the superconducting intercalation complex Tas₂(pyridine) 1/2
- [48] Young, B.-L. et al. Probing The Bulk Electronic States of Bi₂Se₃ Using Nuclear Magnetic Resonance. *Phys. Rev. B* **86**, 075137 (2012)
- [49] Fal'ko, V. & Jungwirth T. Orbital effect of an in-plane magnetic field on quantum transport in chaotic lateral dots. *Phys. Rev. B* **65**, 081306 (2002)
- [50] Taskin, A.A., Legg, H.F., Yang, F. et al. Planar Hall effect from the surface of topological insulators. *Nat Commun* **8**, 1340 (2017).

- [51] Zhu, X., Cao, Y., Zhang, J., Plummer, E. W. & Guo, J. Classification of charge density waves based on their nature. *Proc. Natl Acad. Sci. USA* **112**, 2367–2371 (2015).
- [52] Chiatti, O. *et al.* 2D layered transport properties from topological insulator Bi_2Se_3 single crystals and micro flakes. *Sci Rep* **6**, 27483 (2016).
- [53] Martinez, G. *et al.* Determination of the energy band gap of Bi_2Se_3 . *Sci Rep* **7**, 6891 (2017).
- [54] Zhu, X., Guo, J., Zhang, J., Plummer, E.W., *Advances in Physics: X*, vol 2, issue 3, pp. 622-640 (2017)
- [55] Nisison, D. M. *et al.* Nuclear magnetic resonance as a probe of electronic states of Bi_2Se_3 . *Phys. Rev. B* **87**, 195202 (2013)